Applied Catalysis B: Environmental 84 (2008) 21–29

Contents lists available at ScienceDirect

Applied Catalysis B: Environmental

journal homepage: www.elsevier.com/locate/apcatb

Cu–Ce mixed oxides supported on Al-pillared clay: Effect of method of preparation on catalytic activity in the preferential oxidation of carbon monoxide

Veda Ramaswamy [a,*], Sachin Malwadkar [b], Satyanarayana Chilukuri [b,**]

[a] Chemical Physics Laboratory, Central Leather Research Institute, Adyar, Chennai 600020, India
[b] Catalysis Division, National Chemical Laboratory, Pune 411008, India

ARTICLE INFO

Article history:
Received 3 May 2007
Received in revised form 12 February 2008
Accepted 15 February 2008
Available online 29 February 2008

Keywords:
Alumina-pillared clay
$CuO–CeO_2$
Clay-supported $CuO–CeO_2$
PROX of CO

ABSTRACT

The possibility of using Al-pillared montmorillonite (Al-PILC) clay as a high-surface-area support for $CuO–CeO_2$-based catalysts has been investigated. The preparation of the samples was done by three different methods, *viz.*, amorphous citrate route (ACR), deposition precipitation (DP) and wet impregnation method (WIM). Samples with different $CuO–CeO_2$ loadings (10–50 wt.%) were prepared by each of the three methods. The catalytic activity of these samples was investigated for the preferential oxidation (PROX) of carbon monoxide (CO) in excess of H_2. The samples prepared by DP and WIM methods show better activity than the samples prepared by ACR method. At low Cu content, the samples prepared by DP method have a slight edge over samples prepared by WIM method. The DP-30 sample shows a very high CO conversion of 96.1% at 423 K. A higher dispersion of $CuO–CeO_2$ on pillared montmorillonite clay and better reducibility of copper oxide species may be responsible for the good activity of these samples even at lower reaction temperatures. A higher O_2/CO ratio increased the CO conversion but led to a reduction in oxidation selectivity. No methanation of CO or CO_2 was observed at the reaction temperature. These $CuO–CeO_2$/Al-PILC samples could be considered as comparable in performance with supported noble metal catalysts for the preferential oxidation of CO in excess hydrogen.

1. Introduction

Pillared interlayered clays (in short, PILCs) are a class of molecular-sieve-like materials that have large pores, high surface areas, strong acidity accompanied by fairly good thermal stability [1]. Traditionally, pillared clays and transition metal incorporated pillared clays have been used in a variety of reactions such as alkylation, cracking, dehydrogenation and oxidation reactions [2–5]. In recent years, these solids have been used as catalytic supports for clean technology applications such as DeNO*x* [6]. To our knowledge, pillared clays have not been reported as supports for $CuO–CeO_2$ catalysts for the preferential oxidation (PROX) of carbon monoxide (CO).

The PROX reaction has been extensively investigated [7–13] for processing of H_2 rich reformates to use them as feeds for PEM fuel cells. However, in most of the studies, the reaction feeds used were not representative [14] of reformates that exit a water gas shift (WGS) reactor (CO, CO_2, H_2, CH_4 and H_2O). Presence of some of the reformate components in the mixture (typically water and CO_2) can alter the reaction rates [15], selectivity and in most cases the durability of the catalyst. Among the catalysts used for PROX reaction, noble metal catalysts [16], particularly Pt- and Au-based catalysts are perhaps the most prominent [17–21]. However, the stability of Au supported on various oxides/mixed oxides was suspect, as they deactivated in the presence of CO_2 and/or water. Carbonate formation was reportedly responsible for CO_2 poisoning [17]. Whereas, a recent report suggests that hydrogen in reactant stream enhances the CO oxidation rate over Au supported on alumina [18]. Although Au-based catalysts work at lower temperatures, they require high metal loading (~5 wt.%) and are not very active at high space velocities [19]. On the other hand, supported Pt catalysts show very good activity [20], while H_2 consumption was lower, but maximum conversions could be reached only at higher reaction temperatures. However, at higher temperatures, CO oxidation selectivity was low leading to undesirable combustion of hydrogen. The presence of CO_2 and steam also affected the performance of Pt catalysts, though to a minor extent, reducing the activity by about 10% [17]. Whereas, iron was reported to promote Pt catalysts leading to high activity at lower temperatures [22–24]. However, the high cost of the

* Corresponding author. Tel.: +91 44 2442 0413; fax: +91 44 2491 1589.
** Corresponding author. Fax: +91 20 2590 2633.
E-mail addresses: veda@clri.info (Veda Ramaswamy), sv.chilukuri@ncl.res.in (S. Chilukuri).

0926-3373/$ – see front matter © 2008 Elsevier B.V. All rights reserved.
doi:10.1016/j.apcatb.2008.02.023

precious metals makes it imperative to develop catalysts that use base metals or oxides. Cerium oxide is used as a promoter in the three-way catalysts (TWC) for automotive emission control. CuO–CeO_2 exhibits significant activity in the oxidation of CO [12]. The well-known enhancement of oxidation activity of copper, when supported on reducible oxides like CeO_2, was attributed to a "synergistic" effect [25,26]. It is proposed that well-dispersed CuO on CeO_2, which is reducible at a lower temperature with respect to bulk CuO, could adsorb CO better. As a result, this catalyst exhibited high activity/selectivity for low-temperature CO oxidation [27–29]. Additionally, it was demonstrated that the redox processes corresponding to the CO oxidation involved the reduction and oxidation of both the copper and the ceria species [30–33]. It was postulated that the presence of copper enhances the redox behavior, the oxygen storage capacity and thermal stability of ceria [34]. Cu–O–Ce phases comprising copper oxide clusters strongly associated with ceria are proposed as the active sites for the preferential oxidation of CO [35].

This paper is concerned with the possibility of using alumina-pillared clays (Al-PILC) as support for CuO–CeO_2-based catalysts, as Cu–O–Ce phases are expected to disperse uniformly and offer higher activity on these high-surface-area supports. It is also our aim to study the effect of the method of deposition of CuO–CeO_2 on the physico-chemical properties of the final catalysts. Their activity and selectivity in the PROX reaction were investigated using simulated feeds that are similar in composition processed by a PROX reactor of a fuel processor, which supplies H_2 to a PEM fuel cell. We have observed some good activity for PROX reaction in the case of samples prepared through deposition precipitation (DP) and impregnation methods. Both these catalysts work at reasonably high space velocities and at O_2 to CO mole ratio of 1, whereas Pt-based catalysts usually need O_2/CO ratio >1. The information gained may aid in the development of catalysts that are alternative to precious metal (Pt, Au) catalysts for the low-temperature PROX reaction.

2. Experimental

2.1. Materials and catalyst preparation

$Ce(NO_3)_3{\cdot}6H_2O$ (Loba Chemie, 99.9%), $Cu(NO_3)_2{\cdot}3H_2O$ (Merck, 99%) and citric acid (S.D. Fine Chem., 99.7%) were used as received without further purification. A series of CuO–CeO_2 supported on alumina-pillared montmorillonite clay (herein after designated as CuO–CeO_2–clay) nanocomposites with the composition of $Cu_{0.01}Ce_{0.09}Clay_{0.9}$ to $Cu_{0.05}Ce_{0.45}Clay_{0.5}$ were prepared by three different methods, *viz.*, the amorphous citrate route (ACR), deposition precipitation and wet impregnation method (WIM). One additional composition, $Cu_{0.07}Ce_{0.63}Clay_{0.3}$ was prepared in the case of DP method.

2.1.1. Support

The Na-form of montmorillonite, Kunipia F (Kunimine industries, Japan) was exchanged for Ca^{2+} ions and then used for pillaring with aluminium chlorohydrol [Al_{13}] using ultrasonic technique [36]. Calcium exchange was carried out by stirring the clay with 0.1 M $Ca(NO_3)_2$ for 6 h at 353 K. Subsequently, the clay was filtered, washed with deionized water and air-dried. An aqueous solution of chlorohydrol $[(Al_{13}O_4\ (OH)_{24}(H_2O)_{12}]^{7+}$ from Reheis Inc., U.S.A. was mixed with clay suspension in water (5%) so as to provide 20 mequiv. of $Al^{3+}\ g^{-1}$ of clay. The mixture was agitated in an ultrasonic bath (ELMA Ultrasonic bath MDL T 660/H operating frequency 35 kHz) at ambient temperature (300 K) for 20 min [36]. The product was filtered, washed with de-ionized water till free of chloride ions and air-dried. The sample was calcined at 673 K in a programmable furnace at a heating rate of 5 K min^{-1} for 6 h. This sample was used as support for further loading of CuO–CeO_2 by different methods.

2.1.2. Preparation of CuO–CeO_2–clay by amorphous citrate route (ACR)

For the preparation of $Cu_{0.01}Ce_{0.09}Clay_{0.9}$ nanocomposite, appropriate amounts of $Ce(NO_3)_3{\cdot}6H_2O$, $Cu(NO_3)_2{\cdot}3H_2O$ and citric acid were dissolved in 10 ml of distilled water. The citric acid to CuO–CeO_2 molar ratio was maintained at 1.2 for all the compositions of the samples. The pillared clay prepared as above (Section 2.1.1) was dispersed in this solution. It was slowly evaporated on a hot plate till it was completely dried to form a sticky solid. The dried material was powdered gently in a mortar and calcined in air at 673 K for 6 h to yield the final catalyst. The calcined material was yellow in colour. A number of samples varying in CuO–CeO_2 concentrations from 10 to 50 wt.% were prepared using the above procedure and designated as ACR-10, ACR-20, ACR-30, ACR-40 and ACR-50, respectively.

2.1.3. Preparation of CuO–CeO_2–clay by deposition precipitation method (DP)

For the preparation of $Cu_{0.01}Ce_{0.09}Clay_{0.9}$, appropriate amounts of $Ce(NO_3)_3{\cdot}6H_2O$ and $Cu(NO_3)_2$ were dissolved in 10 ml of distilled water. Required amount of pillared clay was dispersed in this solution and mixed thoroughly with a magnetic stirrer. To this, 0.1 M KOH was added drop wise with continuous stirring at ambient temperature, till complete precipitation (pH 10) was achieved. Subsequently, the precipitate was filtered and washed several times with distilled water to remove the potassium ions and then dried in air at 373 K. The dried samples were calcined at 673 K for 8 h to obtain the final catalyst. The samples prepared were labeled as DP-10, DP-20, DP-30, DP-40, DP-50 and DP-70 based on the wt.% of CuO–CeO_2 content in the sample.

2.1.4. Preparation of CuO–CeO_2–clay by wet impregnation method (WIM)

For the preparation of $Cu_{0.01}Ce_{0.09}Clay_{0.9}$, required amounts of $Ce(NO_3)_3{\cdot}6H_2O$ and $Cu(NO_3)_2{\cdot}3H_2O$ were dissolved in 10 ml of distilled water. To this solution, the pillared clay was added under continuous stirring. After stirring for 3 h, the water was slowly evaporated on a hot plate with continuous stirring until it was completely dried. The solid material was further dried overnight in air at 373 K. The dried material was calcined under air flow at 673 K for 8 h to get the final catalyst. The samples prepared were labeled as WIM-10, WIM-20, WIM-30, WIM-40 and WIM-50 based on the wt.% of CuO–CeO_2 content in the sample.

2.1.5. Catalyst characterization

The powder X-ray diffraction measurements were carried out using a Philips X'Pert Pro diffractometer, equipped with a Ni-filtered Cu Kα (λ = 1.5406 Å, 40 kV, 30 mA) radiation. The sample was mounted on a glass plate and the data were collected in the 2θ range of 2.5–85° with a step size of 0.02° and a scan rate of 2° min^{-1}. The average crystallite size of ceria was determined from the broadening of the XRD peaks corresponding to the (1 1 1) reflection of ceria, using the Debye–Scherrer equation [37].

Diffuse reflectance UV–visible (DRUV–vis) spectra of the solid samples were recorded on a Shimadzu UV2101 spectrophotometer in the diffuse reflectance mode in the 200–900 nm region. The baseline was recorded using spectral grade $BaSO_4$ as the reference material.

Temperature-programmed reduction (TPR) experiments were performed using a Micromeritics Autochem 2910 instrument. Prior

to reduction, a weighed amount of the sample (200 mg) was placed in a quartz reactor, pretreated in the flow of argon (99%) at 773 K for 2 h (ramp rate of 10 K min^{-1}) and cooled to room temperature. Followed by this, a gas mixture containing 5% H_2 in argon was passed (25 ml min^{-1}) through the sample and the temperature was raised to 973 K at a heating rate of 10 K min^{-1}. Thermal conductivity detector after calibration was employed to measure the volume of hydrogen consumed during the reduction process.

2.1.6. Catalytic activity

Preferential oxidation of CO was carried out in a fixed bed, down flow, glass reactor (i.d. = 15 mm). About 0.5 ml (450 mg) of catalyst diluted with 1 ml of inert material was sandwiched between two quartz-wool plugs. The sample was pressed into pellets, up to a pressure of 10 tons, crushed and sieved to 10–20 mesh size. The reactor was placed in a furnace, which is controlled by a PID programmer, and the bed temperature was monitored using a separate thermocouple. Prior to the reaction, the sample was activated in situ at 673 K in air for 3 h and brought to the reaction temperature. A synthetic gas mixture containing H_2 (74.05%), CO (0.5%), CH_4 (2.05) and CO_2 (23.40%) was fed using a mass flow controller (Bronkhorst, Hi Tech) at a desired flow rate (GHSV = 5000–30,000 h^{-1}). This was mixed with the required amount of air (O_2/CO = 0.5–2.0), sent with the help of another mass flow controller. For experiments involving steam (26.66 kPa), water was pumped to a pre-heating zone using a high precision syringe pump (ISCO 500D), wherein the feed gas was mixed with the steam. The dry product gas mixture, after passing through a gas–liquid separator, was analyzed online using a GC (CHEMITO 8610) equipped with two detectors (FID and TCD) and a methanator that can estimate very low concentrations (ppm) of CO detected as CH_4 using FID. Methane present in the feed is detected by TCD independently. An infrared-based gas analyzer (Fuji Electric) was also used in series for real time monitoring of CO, CO_2, CH_4 and O_2 accurately. Spherocarb column (1/8 in. diameter, 8 ft length) was used for achieving base line separation of the gas components analyzed using a thermal conductivity detector. A certified calibrated gas mixture was used as reference to estimate the concentration of gases. Conversions of CO and oxidation selectivity were calculated as

$$\text{CO conversion} = \left[\frac{CO_{in} - CO_{out}}{CO_{in}}\right] \times 100,$$

$$\text{CO oxidation selectivity} = 0.5 \times \left[\frac{CO_{in} - CO_{out}}{O_{2\,in} - O_{2\,out}}\right] \times 100$$

3. Results and discussion

3.1. Powder X-ray diffraction

Fig. 1 shows powder XRD patterns of CuO–CeO_2–clay nanocomposites prepared using three different methods, ACR, DP and WIM, respectively, with varying CuO–CeO_2 loadings. The (0 0 1) reflection of the Al-PILC (2θ = 5.8–6.2°) in most of the samples was intact indicating the preservation of pillared clay structure. Peaks due to cubic fluorite CeO_2 (PDF-ICDD 34–0394) were seen in all the samples and no characteristic peaks due to crystalline CuO phase (typically at 2θ = 35.5°, 38.7°, 48.7° and 61.5°) were observed indicating the absence of bulk CuO phase (with crystallite size ≥3 nm) in these samples. This suggests that copper oxide is highly dispersed on the CeO_2 surface in all the samples prepared in this study.

Independent of the method of preparation, increasing the concentration of CuO–CeO_2 in the CuO–CeO_2–clay composite resulted in the increased intensity of the (1 1 1) peak of CeO_2 (2θ = 28.54°) with a corresponding decrease in the intensity of the (0 0 1) peak of Al-PILC. The CeO_2 peaks were found to be sharper and narrower for the samples prepared by WIM method. The crystallite size calculated by the Scherrer equation using the FWHM of the (1 1 1) peak of CeO_2 was found to depend on the method of preparation and it increased in the order, ACR < DP < WIM (Table 1). The crystallite size of the ceria phase (≤3 nm size) in the samples prepared by the ACR technique could not be calculated because of the very broad and diffuse nature of

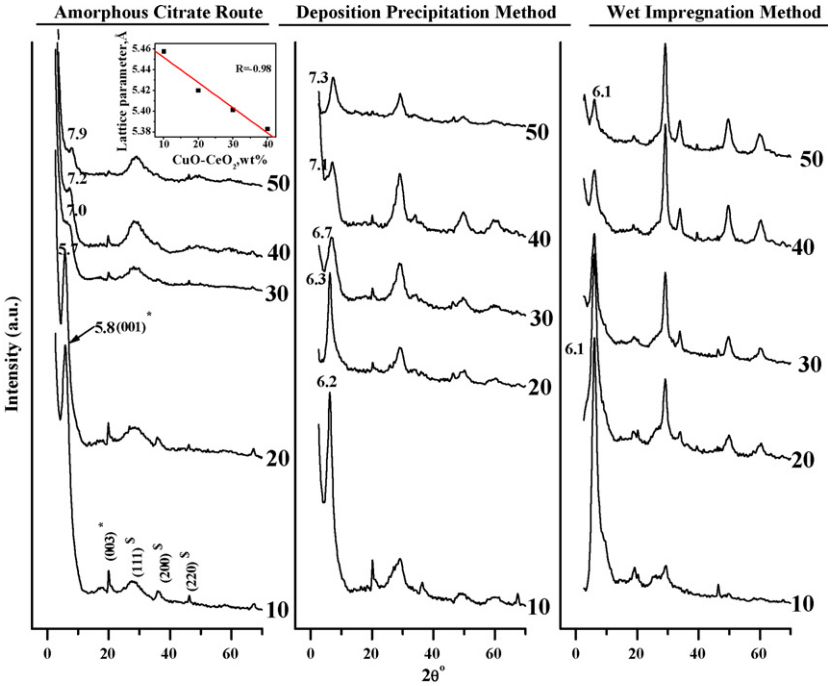

Fig. 1. Powder XRD patterns of the CuO–CeO_2–clay samples prepared by different methods. Inset shows the lattice contraction with increase in Cu concentration in ACR samples.

Table 1
Crystallite size of CeO_2 from XRD data using (1 1 1) peak in CuO–CeO_2–clay nanocomposites

CuO–CeO_2 content in Al-PILC	Crystallite size (CeO_2) (nm)		
	ACR	DP	WIM
10	–	3	5
20	–	3	5
30	–	3	5
40	–	3	6
50	–	3	6

the peak indicating that the ceria was well dispersed on the clay matrix. In the samples prepared by DP method, the CeO_2 (1 1 1) peak was very broad indicating the nanocrystalline nature of the oxide particles. Crystallite size of ceria was found to be larger (5–6 nm) in the samples prepared by wet impregnation method than that of the samples prepared by ACR or DP method ($\leq$3 nm).

Upon incorporation of CuO–CeO_2 in the alumina-pillared clay structure, the low angle reflections shifted to higher angles in ACR and DP samples, while there was no change in WIM samples. A sharp decrease in the intensities of the Al-PILC (0 0 1) peak was observed in all the samples. The shift in the 2θ value of the (0 0 1) reflection is likely due to the X-ray scattering of the confined CuO–CeO_2 nanocrystals, while the decrease in the intensity is due to the reduced concentration of the pillared clay in the composites. Wang et al. [38] and Sauer et al. [39] have also observed this behavior in the samples of TiO_2/ZrO_2 incorporated in SBA-15 and MCM-41 samples. In the samples prepared by the ACR method, the 2θ shift and the decrease in the intensity of the Al-PILC (0 0 1) peak were more prominent. The nanocomposites prepared by DP and WIM methods do not show any shift in the 2θ value of the (1 1 1) reflection of CeO_2, while the samples prepared by ACR method show a shift to higher angles. This shift is probably due to the incorporation of Cu in the CeO_2 lattice. The inset in Fig. 1 shows the contraction of the unit cell parameter with increase in Cu concentration indicating that isomorphous substitution of Ce^{4+} by Cu^{2+} in the ceria lattice in ACR samples.

3.2. DRUV–vis spectroscopy

In order to understand the nature of the copper species present in the samples prepared by different methods, UV–vis diffuse reflectance spectroscopy was used. Fig. 2a shows the UV–vis spectra of the CuO–CeO_2–clay nanocomposites containing 10, 20, 30, 40 and 50 wt.% CuO–CeO_2 samples and Fig. 2b shows the representative deconvoluted UV–vis spectra of 50 wt.% CuO–CeO_2 samples prepared by all the three different methods. A wide band in the region of 215 and 350 nm was attributed to the Ce^{4+}–O^{2-} charge transfer [40]. The former is a specular reflectance band developing from the surface sites while the latter is a diffuse reflectance band arising from bulk ceria. Apart from this, the clay nanocomposite samples prepared by DP and WIM methods revealed a broad band in the 400–500 nm range. Praliaud et al. [40] assigned this band to the three-dimensional Cu^{+} species present in the CuO matrix. Bulk-like $CuAl_2O_4$ species also shows strong absorption in this region [41]. However, we have not observed any XRD peaks corresponding to $CuAl_2O_4$ in our samples. Hence, we attribute the broad band in the 400–500 nm range to Cu^{+} species. The samples ACR-10 to ACR-30 did not show absorption in this region, while a small peak in this region is observed for samples ACR-40 and ACR-50, which contain a higher concentration of copper. Remarkably, this band is easily discernible in the WIM samples even at the lowest concentration of Cu. A broad band in the visible region (600–900 nm) was seen in samples prepared by different methods. Absorption in this region is attributed to the d–d transition of Cu^{2+} situated in octahedral environment with O_h symmetry [40]. This band is the most prominent in the samples prepared by WIM even with low Cu content. This signifies that majority of the Cu^{2+} is present in the octahedral coordination in the WIM sample.

3.3. Temperature-programmed reduction

The TPR profiles of CuO–CeO_2–clay composites (30 wt.% CuO–CeO_2) prepared by the three methods are presented in Fig. 3a. Representative profiles of the samples containing 10–50 wt.% of CuO–CeO_2 on clay prepared by DP method are shown in Fig. 3b. The method of preparation influences the nature of oxides that undergo reduction, *viz.*, CuO and CeO_2, while Al-PILC is passive to H_2 treatment. Bulk CuO exhibits a single reduction peak with a T_{max} at 539 K (Fig. 3c), while pure CeO_2 undergoes reduction in the temperature range, 700–1050 K, generally with two temperature maxima attributed to the reduction of surface Ce^{4+} followed by reduction of bulk ceria, respectively [29]. The TPR data of CuO-supported in Al-PILC (Fig. 3c) indicate that the T_{max} of reduction is retained.

The TPR profiles given in Fig. 3a (for samples ACR-30, DP-30 and WIM-30) can be considered as the fingerprints of the samples, as the concentration of reducible oxides varies considerably, discerned from the H_2 consumption for the total reduction process in the given temperature range. The H_2 consumption is higher for WIM-30 sample (414.4 μmol g^{-1}) compared to DR-30 (266.5 μmol g^{-1}) and ACR (185.6 μmol g^{-1}). In general, the profiles show three reduction maxima in the range, 423–448, 500–524 and 700–810 K. The low-temperature peak, common to all the three samples, is attributed to finely dispersed CuO, whose concentration is very low in ACR sample compared to the other two samples. These could be surface-bound CuO species which are easily reduced and probably in close contact with ceria. The reducibility of such CuO species in the three samples is in the order, WIM > DP > ACR. The observed T_{max} for this type of CuO species is lower than that for the bulk CuO. The lower temperature required for the reduction as compared to pure CuO suggests that these Cu species are present in highly isolated state while interacting strongly with the support. In the ACR technique, citric acid is used as a complexing agent as well as a fuel that generates heat on calcination, which can lead to sintering of Cu as well as formation of solid solution of Cu in ceria, such as $Cu_xCe_{1-x}O_2$. This is evidenced also from XRD data. From the intensity of this low-temperature peak, such reducible CuO species in ACR-30 sample is much lower compared to other two samples.

The second reduction process centers on a temperature maxima of 500–524 K for the three samples. This temperature is closer to T_{max} observed for pure CuO and hence may be assigned to bulk-like CuO or clustered CuO species that are loosely bound to ceria or the support and somewhat more difficult to reduce. In ACR-30 sample, such CuO species are more difficult to reduce than in the other two samples, for probably the same reason as given earlier.

The high temperature reduction process (T_{max} = 700–810 K) (better seen in WIM-30 and DP-30 samples) is associated with the reduction of ceria, the surface Ce^{4+} undergoing reduction first followed by the bulk CeO_2 in this temperature range and the reduction may be facilitated by the presence of Cu [42]. From the intensity of this reduction peak, it can be inferred that the concentration of such reducible ceria in these three samples is in the order, WIM $\gg$ DP > ACR. In the latter sample, the formation of the solid solution such as $Cu_xCe_{1-x}O_2$ may inhibit the reduction of Ce^{4+} ions in the surface. The bulk ceria reduction is normally seen at still higher temperatures (>1000 K), not covered under our TPR experiments.

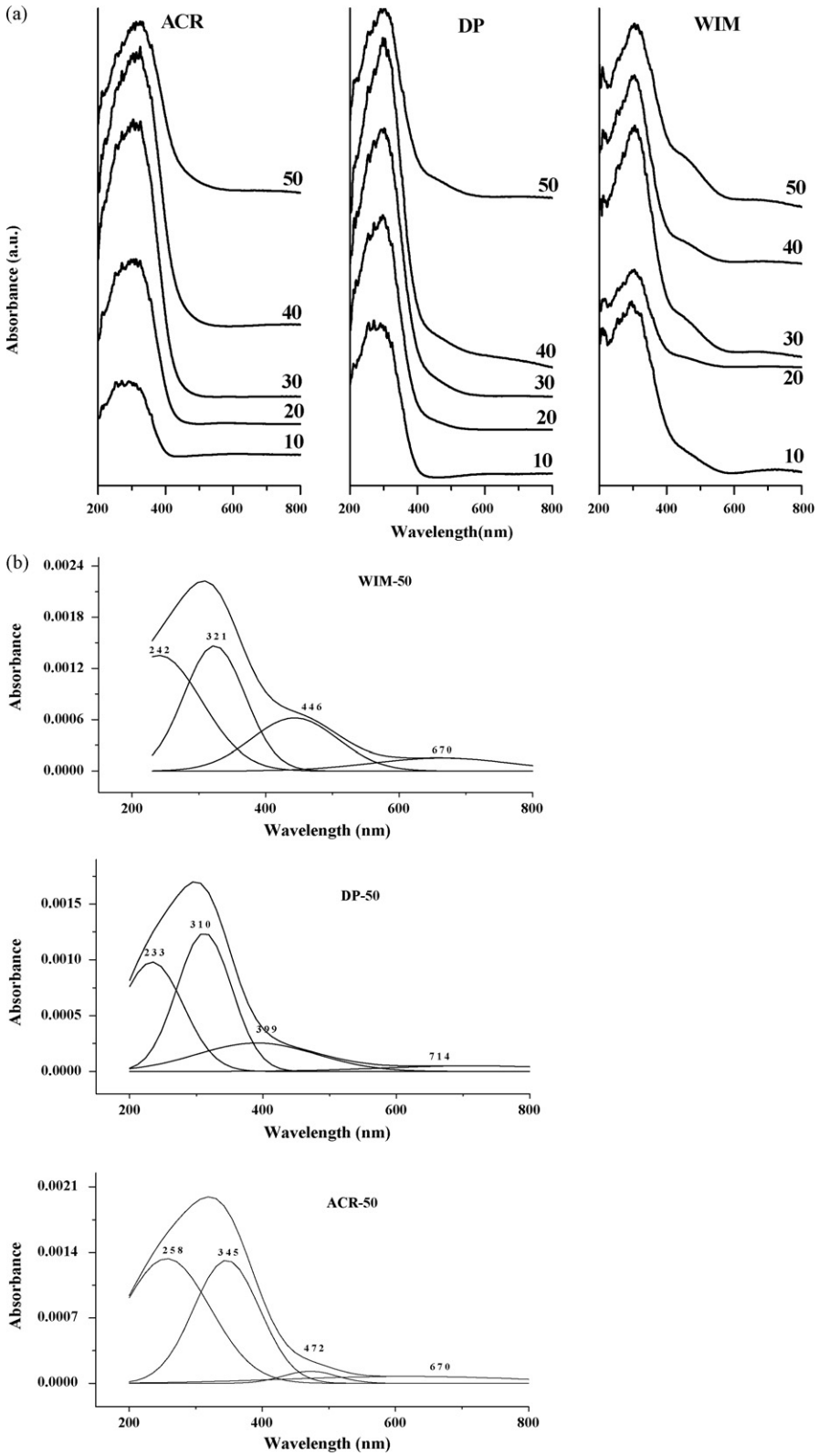

Fig. 2. (a) DRUV–vis spectra of the CuO–CeO_2 clay nanocomposites of different Cu concentration prepared by different methods. (b) Deconvoluted DRUV–vis spectra of 50 wt.% CuO–CeO_2 clay nanocomposites prepared by different methods.

The effect of the concentration of Cu on the nature of Cu species formed is seen in Fig. 3b, where the TPR profiles of the samples prepared by DP method with different contents of CuO–CeO_2 are presented. At lower concentration of CuO (DP-10), the TPR profile shows three peaks, *viz.*, a shoulder at 474 K and two peaks at 561 and 802 K. The shoulder at 474 K is due to the reduction of highly dispersed CuO on the CeO_2 surface and the peak at 561 K is due to the reduction of CuO clusters present in the CuO–CeO_2–clay nanocomposites. With increase in CuO content in the CuO–CeO_2–clay nanocomposites, the low-temperature peak at 474 K shifted to

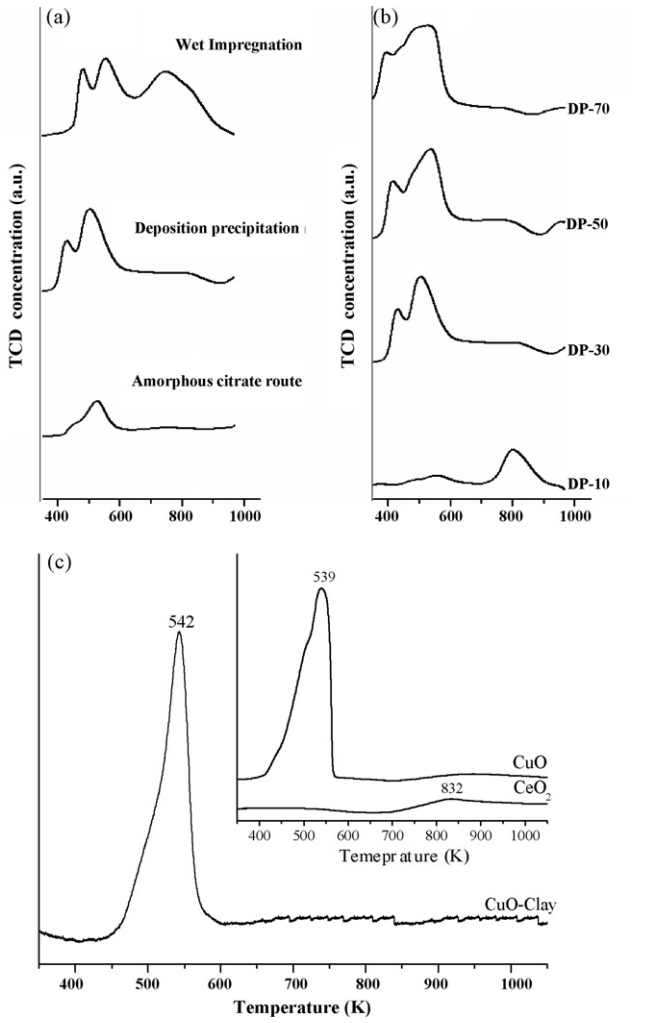

Fig. 3. (a) TPR profiles of the 30 wt.% CuO–CeO_2–clay nanocomposites prepared by different methods. (b) TPR profiles of the CuO–CeO_2–clay nanocomposites prepared by deposition precipitation (DP) method with different CuO–CeO_2 contents. (c) TPR profiles of pure CuO, ceria and CuO–Al-PILC samples.

still lower temperature. In contrast, the peak at 561 K has slightly shifted to a higher temperature, at the same time, the peak becoming relatively broader. The broadening of the peak with increasing concentration of CuO can be attributed to the formation of relatively larger CuO crystallites (which are XRD amorphous) accompanied by poor dispersion of CuO on the surface of ceria–Al-PILC. In general, the total reducible CuO increases with increasing Cu content up to about 50% in samples prepared by DP method. The DP-10 sample shows a peak with a T_{max} at 810 K, which is associated with the reduction of surface Ce^{4+} ions. In this sample, most of ceria is well dispersed on clay and surface-bound. In other samples, as the total CuO–CeO_2 content increases, the concentration of surface ceria decreases. The reduction of bulk ceria takes place at still higher temperature not recorded in the given TPR profiles.

3.4. Catalytic activity of CuO–CeO_2–clay composites in preferential oxidation (PROX) of CO

The activity of the catalysts was tested in the preferential oxidation of CO, using CO containing gas mixture that is rich in hydrogen. The effect of the method of preparation is shown in Fig. 4 for 30 and 50 wt.% CuO–CeO_2–clay nanocomposites at a reaction temperature of 423 K. The 30 wt.% CuO–CeO_2–clay sample prepared by ACR method (ACR-30) gave lowest activity (CO conversion of 19.1%) amongst the catalysts prepared by three methods. The sample DP-30 shows much better PROX activity with a maximum CO conversion of 96.1% at 423 K along with oxidation selectivity of 48.1%. The sample WIM-30 also gave reasonably good performance with a CO conversion of 92.9% with good oxidation selectivity (52%). The CuO–CeO_2 mixed oxides were reported to be remarkably active and promising for PROX reaction [7,29,35,42–43]. Our results further support the efficacy of CuO–CeO_2 when dispersed in a high-surface-area matrix such as Al-PILC for this reaction. In addition, the present study also shows that the preparation method has a strong influence on the catalytic performance [44–46].

Our results show that the samples prepared by the DP and WIM methods are more active and selective for PROX than those prepared by ACR method. Among the DP and WIM methods, samples prepared by DP method are relatively more active compared to WIM samples, though the latter offer better oxidation selectivity. Samples prepared by ACR method (e.g., 30 wt.% CuO–CeO_2), on the other hand, fared very poorly in terms of CO conversion (19.1% for ACR-30) as well as in oxidation selectivity (34.1%, Fig. 4). ACR-50 catalyst, with higher CuO–CeO_2 content, on the other hand gave better CO conversion and also slightly improved oxidation selectivity among the ACR samples. A marginal fall in CO oxidation selectivity was noticed with increasing CuO–CeO_2 content for DP and WIM series of samples (DP-50 and WIM-50). While catalysts prepared by DP method offer better activity, oxidation selectivity was marginally better on the catalysts prepared through WIM method. Luo et al. reported better performance for copper catalysts prepared by impregnation method [28]. The superior performance of WIM and DP series of samples may be attributed to better reducibility of copper species (vide TPR results) in these samples [28]. This in turn could be attributed to a higher fraction of easily reducible CuO present on the surface on these catalysts as compared to ACR samples. In the case of ACR technique, the majority of copper must be present as difficult to reduce form of Cu in the fluorite lattice (as Cu–ceria solid solution). TPR profiles in Fig. 3a and the lower H_2 consumption in the ACR-30 sample reflects this very clearly.

The catalytic activity of CuO–CeO_2–clay nanocomposites prepared through three different routes was explored further under different reaction conditions, *viz.*, reaction temperature, O_2/CO ratio, presence of steam and variation of space velocity. Influence of copper metal loading on PROX performance was also investigated to optimize the concentration of copper.

At high temperatures, CO concentration at the outlet gradually increases as a result of oxidation of H_2 against the desired selective CO oxidation. This leads to undesired consumption of hydrogen, thus lowering oxidation selectivity as shown in Fig. 5 for DP-50 sample. The influence of Cu content on CO conversion and oxidation selectivity for the samples prepared by DP method is shown in Fig. 6 at a reaction temperature of 423 K. Increase of copper content in the catalysts led to an increase in CO oxidation activity initially, while further increase in copper content led to a fall in both CO conversion and oxidation selectivity. The maximum CO conversions may be attained at slightly different temperatures which may be different for each catalyst. The drop in CO oxidation activity may be due to the relative increase in particle size of copper (which is XRD amorphous) and the formation of bulk CuO, at higher Cu loadings. The finely dispersed CuO on CeO_2 is responsible for the CO oxidation at low temperatures, while the bulk CuO hardly contributes to the overall activity [45,47,48]. This is reflected in TPR profiles of these samples (Fig. 3b). At increased space velocities, CO conversion fell marginally, with the fall being considerable at higher space velocities. However, it is still

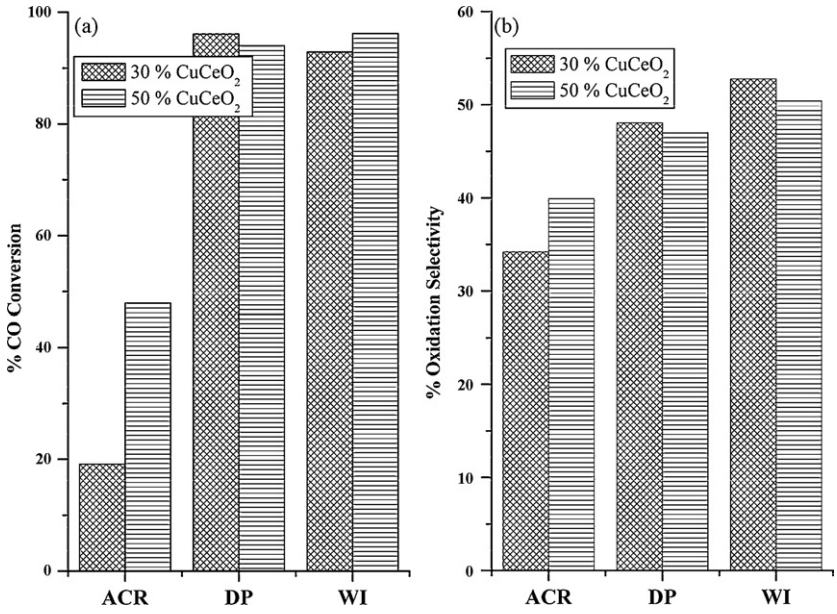

Fig. 4. Influence of the method of preparation on PROX performance over CuO–CeO_2–clay nanocomposites. Reaction conditions: catalyst = 0.5 cm^3; O_2/CO = 1.0; GHSV = 10,000 h^{-1}; temperature = 423 K. Feed: H_2 (74.05%), CO (0.5%), CH_4 (2.05) and CO_2 (23.40%).

remarkable that this catalyst gave closer to 90% conversion at a space velocity of 25,000 h^{-1} (Fig. 7). The variation of space velocity has only marginal influence on CO oxidation selectivity, as it was enhanced only to a small extent. A marginal increase in the reaction temperature (about 5 K) was found to compensate for the loss in the CO conversion at higher space velocities.

Stoichiometrically, one mole of CO requires half a mole of O_2 (O_2/CO − 0.5), but at this ratio the conversion is usually lower than that desirable, thus needing excess oxygen (O_2/CO ≥ 1.0) to achieve >98% conversion. Close to 100% CO conversion is the primary requisite for any PROX catalyst in a fuel processor. However, the excess oxygen (air) leads to a reduction in oxidation selectivity. Fig. 8 shows the effect of O_2/CO ratio on PROX activity and selectivity over DP-50 catalyst. The CO oxidation increased with increasing O_2/CO, but the oxidation selectivity was lowered, as the excess oxygen available in the system was used for non-selective oxidation of H_2.

Usually, the reformate gas mixture that exits WGS reactor contains ≥20 vol.% water and 15–25 vol.% CO_2. However, in many earlier reports feeds that are free of water (steam) and CO_2 have been employed. In fact, many of the studies report reduction in CO oxidation activity in the presence of H_2O and/or CO_2. In principle, the presence of H_2O leads to a reduction in CO conversion, while the presence of CO_2 drives reverse water gas shift reaction. Similarly, a good PROX catalyst should not promote methanation. Fig. 9 shows the influence of water (steam) on the PROX reaction. For water containing feeds, substantial reduction in CO oxidation activity was observed, while slightly better oxidation selectivity was observed in the presence of steam. Water was found to enhance the CO oxidation activity over gold catalysts, as it helps to decompose the carbonates formed on the catalyst during the reaction [21]. However, the influence of water varies with one support to another. The adverse affect of water and CO_2 was also observed by Avgouropoulos et al. for CuO–CeO_2 catalysts prepared

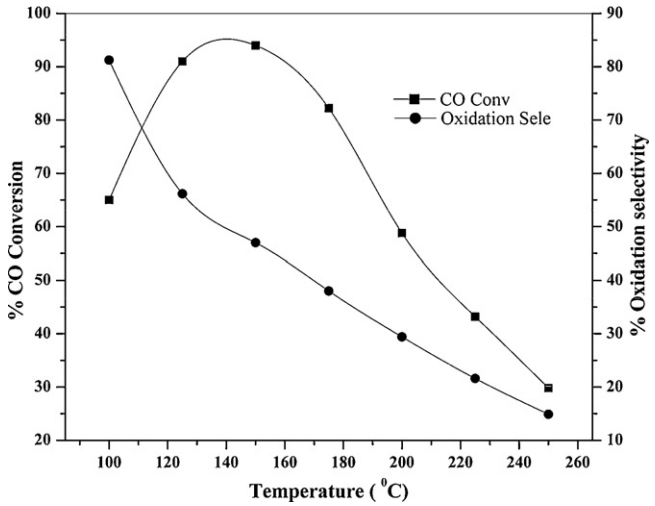

Fig. 5. Preferential oxidation of CO over DP-50 catalyst as a function of temperature. Reaction conditions: catalyst = 0.5 cm^3; O_2/CO = 1.0; GHSV = 10,000 h^{-1}. Feed: H_2 (74.05%), CO (0.5%), CH_4 (2.05) and CO_2 (23.40%).

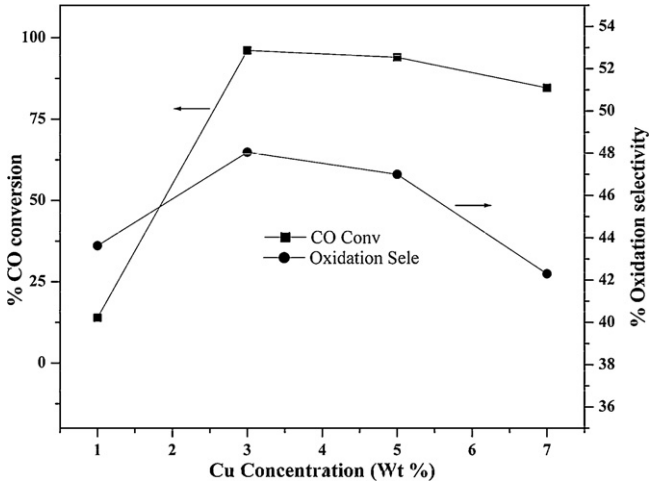

Fig. 6. Influence of Cu concentration on CO conversion and oxidation selectivity over DP samples. Reaction conditions: catalyst = 0.5 cm^3; O_2/CO = 1.0; GHSV = 10,000 h^{-1}; temperature = 423 K. Feed: H_2 (74.05%), CO (0.5%), CH_4 (2.05) and CO_2 (23.40%).

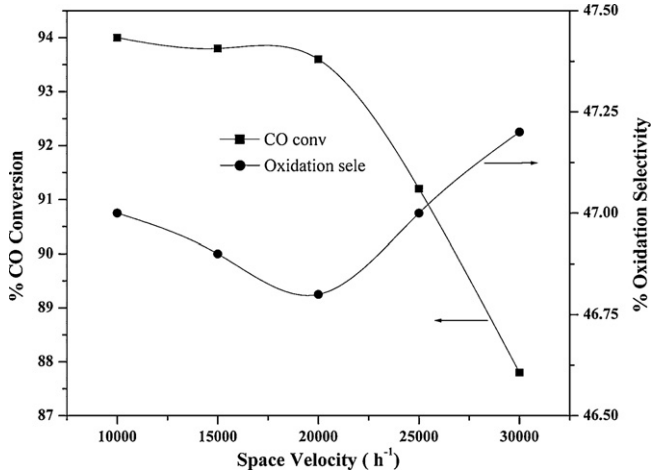

Fig. 7. Effect of space velocity (GHSV) on CO conversion and oxidation selectivity over DP-50 CuO–CeO_2–clay nanocomposites. Reaction conditions: catalyst = 0.5 cm^3; O_2/CO = 1.0; temperature = 423 K. Feed: H_2 (74.05%), CO (0.5%), CH_4 (2.05) and CO_2 (23.40%).

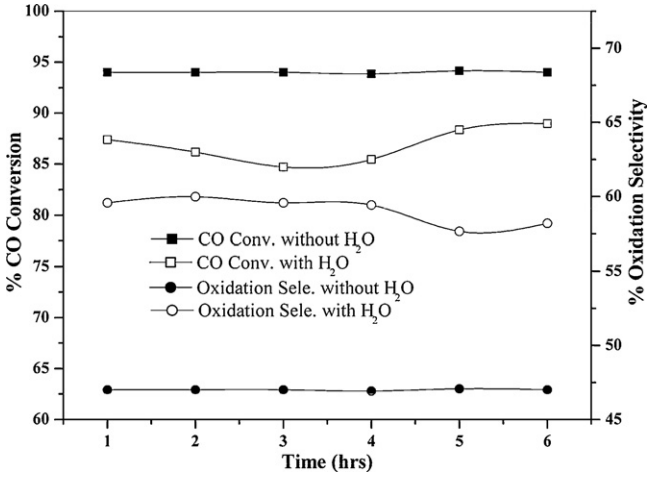

Fig. 9. Effect of water on the conversion of CO and oxidation selectivity over DP-50 CuO–CeO_2–clay nanocomposites. Reaction conditions: catalyst = 0.5 cm^3; O_2/CO = 1.0; GHSV = 10,000 h^{-1}; temperature = 423 K. Feed: H_2 (74.05%), CO (0.5%), CH_4 (2.05) and CO_2 (23.40%).

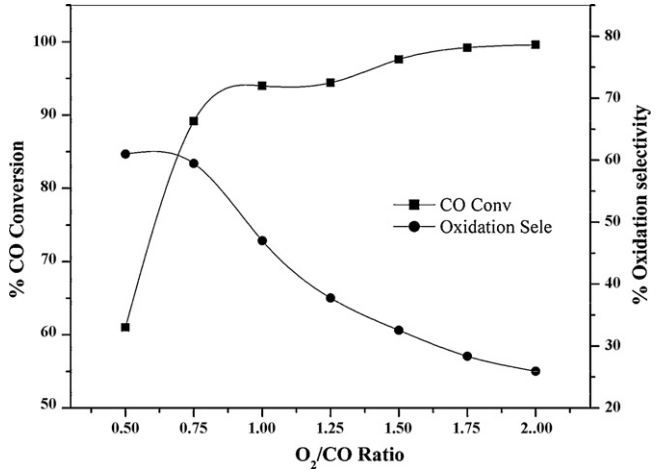

Fig. 8. Effect of O_2/CO ratio on the CO conversion and oxidation selectivity over DP-50 catalyst. Reaction conditions: catalyst = 0.5 cm^3; GHSV = 10,000 h^{-1}; temperature = 423 K. Feed: H_2 (74.05%), CO (0.5%), CH_4 (2.05) and CO_2 (23.40%).

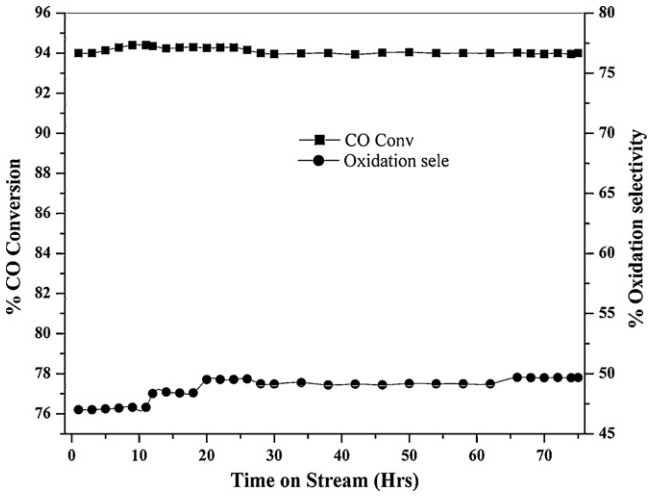

Fig. 10. Time on stream behavior of CuO–CeO_2–clay catalyst (DP-50) during preferential oxidation of CO. Reaction conditions: catalyst = 0.5 cm^3; O_2/CO = 1.0; GHSV = 10,000 h^{-1}; temperature = 423 K. Feed: H_2 (74.05%), CO (0.5%), CH_4 (2.05) and CO_2 (23.40%).

Table 2
Comparison of performance of various reported catalysts for preferential oxidation of CO in H_2 rich gas mixtures

Catalyst	Reaction temperature (K)	Conversion of CO (vol.%)	Oxidation selectivity (%)	Contact time (g s cm^{-3})	O_2/CO ratio	CO in feed (vol.%)	Reference
CuO–CeO_2 on pillared clay—DP method	423	96.1	48	0.28	1.00	0.5[a]	This work
CuO–CeO_2 on pillared clay—DP method	423	94.0	47	0.28	1.00	0.5[b]	This work
CuO–CeO_2 on pillared clay—DP method	423	93.6	47	0.14	1.00	0.5[a]	This work
$CuCeO_2$ by UGC	418	96.0	97	0.02	1.00	1%	[27]
$CuCeO_2$ by UGC	438	99.0	65	0.36	1.00	1%[b]	[27]
$CuCeO_2$ by co-precipitation	443	99.0	63	0.36	1.25	1%[b]	[12]
CeO_2 by co-precipitation	398	99.9	70	0.03	1.25	1%	[12]
$CuCeO_2$ by co-precipitation	423	99.7	39	0.60	1.25	0.5[b]	[21]
$CuCeO_2$ by citrate-hydrothermal	448	99.9	70	0.03	1.25	1%[a]	[36]
$CuCeO_2$ by urea nitrates combustion	498	99.9	45	0.03	1.25	1%[a]	[36]
$CuCeO_2$ by impregnation	473	90.0	50	0.03	1.25	1%[a]	[36]
Thermal	448	99.0	85	0.03	1.25	1%	[39]
$CuCeO_2$ by sol–gel method	423	98.0	40	0.03	1.25	1%[a]	[7]
Au–CeO_2	373	100	33	0.06	1.60	0.5[a]	[45]
Pt/Al_2O_3	473	84.0	43	0.06	1.00	1%	[46]
Pt/Al_2O_3 with base metal oxide	363	75.0	80	0.03	0.50	0.1	[16]

[a] With CO_2.
[b] With CO_2 and H_2O.

by citrate-hydrothermal method that otherwise showed a very good activity [45,49].

Fig. 10 shows the time on stream stability of DP-50 catalyst for a reaction period up to 75 h. The CO conversion remained fairly stable, while there was a marked improvement in oxidation selectivity with time on stream. This improvement in selectivity may be attributed to two factors, *viz.*: (i) the catalytic sites that are responsible for non-selective oxidation (oxidation of H_2) are deactivated during the time on stream; (ii) the small amount of water formed initially from the oxidation of H_2 probably helps in suppressing further oxidation of H_2. The water derived species, such as –OH, on gold catalysts was reported to promote CO oxidation reaction [50,51].

Table 2 presents a comparison of the activity of present clay-supported CuO–CeO_2 catalyst vis-à-vis the results reported on the preferential oxidation of CO by others. For most of the CuO–CeO_2 systems the CO conversion was greater than 95%, while the oxidation selectivity in the range of 39–97%. In our case, though the CO conversion was slightly on the lower side (~96.1%) at 423 K, it is to be noted that ours is a diluted (50%) system and that we have not attempted to achieve maximum conversion, by varying the reaction parameters (temperature, etc.). The oxidation selectivity is also lower than those reported by some of the authors [12,35,45,49]. However, our system differs from those reported, as it contains less amount of CeO_2 which might be playing a vital role in improving oxidation selectivity. Hence, we feel that present clay-supported system is interesting as it gives comparable CO conversion as has been reported for CuO–CeO_2 system, though it needs to be further improved upon by optimizing the Cu and CeO_2 contents.

The oxidation of CO on metals is known to obey a single-site Langmuir–Hinshelwood kinetic model [52] where CO and O_2 compete for the same sites. In the case of metals supported on reducible oxides, similar to the present CuO–CeO_2 system, CO may be adsorbed exclusively on active copper sites while adsorption of O_2 may take place on both the metal (Cu) and support (CeO_2), thus facilitating higher activity on these catalysts. Methanation is a side reaction that takes place on many metal (Co, Ni) supported catalysts in the presence of CO containing H_2 rich feeds [53]. However, no methanation activity was observed for the present catalyst system.

4. Conclusions

This study reports the preparation, characterization and testing of catalytic activity of CuO–CeO_2–clay nanocomposites, prepared by different methods. Of the three different methods used for the preparation of catalysts, deposition precipitation and wet impregnation methods yielded better catalysts. Higher activity of these catalysts is correlated to the better reducibility of copper species as shown by TPR results. Formation of Cu–CeO_2 solid solutions was observed in samples prepared by amorphous citrate route which showed higher reduction temperature for both CuO and ceria. Sample containing 50 wt.% CuO–CeO_2 (DP-50) on Al-PILC exhibited good, stable activity, while the oxidation selectivity improved with time on stream. Increased O_2/CO ratio leads to an improved CO conversion activity, but also results in lowering the oxidation selectivity. The presence of water adversely affected the CO conversion, but it helped in achieving better CO oxidation selectivity. No methanation activity was observed at any reaction conditions on these CuO–CeO_2–Clay catalysts. This study shows the potential of a well-dispersed CuO–CeO_2 catalytic system, which has PROX activity comparable to precious metal catalysts. The performance of the catalyst can be further improved to achieve the desired conversion and oxidation selectivity with further modifications and optimization of the compositions. The low-temperature activity is a positive indication of the same.

Acknowledgements

Authors are grateful to Miss Neelam Jagtap for help in the synthesis of samples and providing UV–vis spectral data. VR thanks the Department of Science and Technology, New Delhi for the financial support.

References

[1] A. Gil, L.M. Gandia, M.A. Vicente, Catal. Rev. Sci. Eng. 42 (2000) 145–212.
[2] M. Raimondo, G. Perez, A. De Stefanis, A.A.G. Tomlinson, Appl. Catal. A 164 (1997) 119–226.
[3] F. González, C. Pesquera, I. Benito, E. Herrero, C. Poncio, S. Casuscelli, Appl. Catal. A 181 (1999) 71–76.
[4] L. Huerta, A. Meyer, E. Choren, Microporous Mesoporous Mater. 57 (2003) 219–227.
[5] L.M. Gandía, M.A. Vicente, A. Gil, Appl. Catal. B 38 (2002) 295–307.
[6] R.Q. Long, R.T. Yang, Catal. Lett. 59 (1999) 39–44.
[7] G. Avgouropoulos, T. Ioannides, Ch. Papadopoulou, J. Batista, S. Hocevar, H.K. Matralis, Catal. Today 75 (2002) 157–167.
[8] G.K. Bethke, H.H. Kung, Appl. Catal. A 194–195 (2000) 43–53.
[9] R.J.H. Grisel, B.E. Nieuwenhuys, J. Catal. 199 (2001) 48–59.
[10] M.M. Schubert, V. Plzak, J. Garche, R.J. Behm, Catal. Lett. 76 (2001) 143–150.
[11] Y.-F. Han, M.J. Kahlich, M. Kinne, R.J. Behm, Phys. Chem. Chem. Phys. 4 (2002) 389–397.
[12] G. Avgouropoulos, T. Ioannides, H.K. Matralis, J. Batista, S. Hocevar, Catal. Lett. 73 (2001) 33–40.
[13] D.H. Kim, M.S. Lim, Appl. Catal. A 224 (2002) 27–38.
[14] Y.-Z. Chen, B.-J. Liaw, C.-W. Huang, Appl. Catal. A 302 (2006) 168–176.
[15] A. Manasilp, E. Gulari, Appl. Catal. B 37 (2002) 17–25.
[16] F. Marino, C. Descorme, D. Duprez, Appl. Catal. B 54 (2004) 59–66.
[17] A. Luengnaruemitchai, D.T. Kim Tho, S. Osuwan, E. Gulari, Int. J. Hydrogen Energy 30 (2005) 981–987.
[18] E. Quinet, F. Morfin, F. Diehl, P. Avenier, V. Caps, J.-L. Rousset, Appl. Catal. B 80 (2008) 195–201.
[19] M.M. Schubert, M.J. Kahlich, H.A. Gasteiger, R.J. Behm, J. Power Sources 84 (1999) 175–182.
[20] O. Korotkikh, R. Farrauto, Catal. Today 62 (2000) 249–254.
[21] M. Haruta, M. Date, Appl. Catal. A 222 (2001) 427–437.
[22] X. Liu, O. Korotkikh, R. Farrauto, Appl. Catal. A 226 (2002) 293–303.
[23] M. Watanabe, H. Uchida, K. Ohkubo, H. Igarshi, Appl. Catal. B 46 (2003) 595–600.
[24] G.W. Roberts, P. Chin, X. Sun, J.J. Spivey, Appl. Catal. B 46 (2003) 601–611.
[25] J.B. Wang, W.H. Shih, T.-J. Huang, Appl. Catal. A 203 (2000) 191–199.
[26] E. Moretti, M. Lenarda, L. Storaro, A. Talon, R. Frattini, S. Polizzi, E. Rodriguez-Castellon, A. Jimenez-Lopez, Appl. Catal. B 72 (2007) 149–156.
[27] J. Xiaoyuan, L. Guanglie, Z. Renxian, M. Jianxin, C. Yu, Z. Xiaoming, Appl. Surf. Sci. 173 (2001) 208–220.
[28] M. Luo, Y. Zhong, X. Yuan, X. Zheng, Appl. Catal. A: Gen. 162 (1997) 121–131.
[29] P. Ratnasamy, D. Srinivas, C. Satyanarayana, P. Manikandan, R. Senthil Kumaran, M. Sachin, V. Shetti, J. Catal. 221 (2004) 455–465.
[30] A. Martinez-Arias, M. Fernández-García, J. Soria, J. Conesa, J. Catal. 182 (1999) 367–377.
[31] A. Martinez-Arias, M. Fernández-García, O. Gálvez, J. Coronado, J. Anderson, J. Conesa, J. Soria, G. Munuera, J. Catal. 195 (2000) 207–216.
[32] J. Wang, S. Lin, T. Huang, Appl. Catal. A: Gen. 232 (2002) 107–120.
[33] G. Jernigan, G. Somorjai, J. Catal. 147 (1994) 567–577.
[34] S. Kacimi, J. Barbier Jr., R. Taha, D. Duprez, Catal. Lett. 22 (1993) 343–350.
[35] Y. Liu, Q. Fu, M.F. Stephanopoulos, Catal. Today 93–95 (2004) 241–246.
[36] S.P. Katdare, V. Ramaswamy, A.V. Ramaswamy, J. Mater. Chem. 7 (1997) 2197–2199.
[37] H.P. Klug, L.E. Alexander, X-ray Diffraction Procedures: For Polycrystalline and Amorphous Materials, John Wiley & Sons, New York, 1974, p. 618.
[38] X. Wang, M.V. Landau, H. Rotter, L. Vradman, A. Wolfson, A. Erenberg, J. Catal. 222 (2004) 565–571.
[39] J. Sauer, F. Marlow, F. Schüth, Phys. Chem. Chem. Phys. 3 (2001) 5579–5584.
[40] H. Praliaud, S. Mikhailenko, Z. Chajar, M. Primet, Appl. Catal. B 16 (1998) 359–374.
[41] R.M. Friedman, J.J. Freeman, J. Catal. 55 (1978) 10–28.
[42] W. Liu, M. Flytzani-Stephanopoulos, J. Catal. 153 (1995) 304–316.
[43] B. Murugan, A.V. Ramaswamy, D. Srinivas, C.S. Gopinath, V. Ramaswamy, Chem. Mater. 17 (2005) 3983–3990;
A. Igarashi, N. Ichikawa, S. Sato, R. Takahashi, T. Sodesawa, Appl. Catal. A: Gen. 300 (2006) 50–57.
[44] G. Avgouropoulos, T. Ioannides, Appl. Catal. A 244 (2003) 155–167.
[45] G. Avgouropoulos, T. Ioannides, H. Martralis, Appl. Catal. B 56 (2005) 87–93.
[46] G. Marban, A.B. Fuertes, Appl. Catal. B 57 (2005) 43–53.
[47] R. Lin, M.-F. Luo, Y.-J. Zhong, Z.-L. Yan, G.-Y. Liu, W.-P. Liu, Appl. Catal. A 255 (2003) 331–336.
[48] X. Zheng, X. Zhang, X. Wang, S. Wang, S. Wu, Appl. Catal. A 295 (2005) 142–149.
[49] G. Avgouropoulos, T. Ioannides, Appl. Catal. B 67 (2006) 1–11.
[50] G.C. Bond, D.T. Thompson, Gold Bull. 33 (2000) 41–51.
[51] H.H. Kung, M.C. Kung, C.K. Costello, J. Catal. 216 (2003) 425–432.
[52] R.J. Farrauto, C. Bartholomew, Introduction to Industrial Catalytic Processes, Chapman & Hall, London, 1997 (Chapters 1, 38, 39).
[53] F. Marino, C. Descorm, D. Duprez, Appl. Catal. B 58 (2005) 175–183.